

**EXPLORING NANOSCALE PHENOMENA BY UTILIZING RESONANCE  
IN SEMICONDUCTOR MATERIALS WITH PLASMONIC AND  
NANOMECHANICAL DEVICES**

**DURGESH BANSWAR**



**DEPARTMENT OF MATERIALS SCIENCE AND ENGINEERING  
INDIAN INSTITUTE OF TECHNOLOGY DELHI  
APRIL 2026**

© Indian Institute of Technology Delhi (IITD), New Delhi, 2026

---

**Exploring Nanoscale Phenomena by utilizing Resonance  
in Semiconductor Materials with Plasmonic and  
Nanomechanical Devices**

by

**Durgesh Banswar**

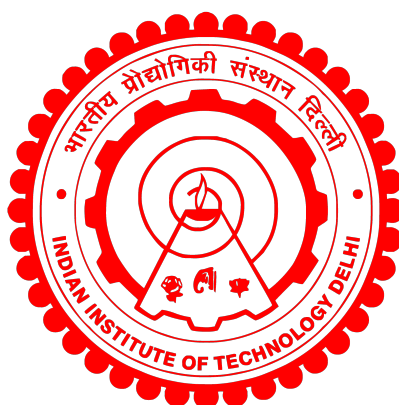
**DEPARTMENT OF MATERIALS SCIENCE AND ENGINEERING**

Submitted

in fulfilment of the requirements of the degree of

**DOCTOR OF PHILOSOPHY**

to the



**INDIAN INSTITUTE OF TECHNOLOGY DELHI**

**April 2026**

---

Dedicated to my beloved Parents and Lord Shiva

**Durgesh Banswar**

April 2026

## **CERTIFICATE**

This is to certify that the thesis entitled **Exploring Nanoscale Phenomena by utilizing Resonance in Semiconductor Materials with Plasmonic and Nanomechanical Devices**, submitted by **Mr. Durgesh Banswar**, to the Indian Institute of Technology Delhi, for the award of the degree of **Doctor of Philosophy (PhD)**, is a bonafide record of the research work done by him under my supervision. The contents of this thesis work, in full or in parts, have not been submitted to any other Institute or University for the award of any degree or diploma.

**Dr. Ankur Goswami**  
Associate Professor  
Department of Materials Science and  
Engineering (DMSE)  
Indian Institute of Technology Delhi,  
Delhi, India

New Delhi  
April 2026

## ACKNOWLEDGEMENTS

I express my heartfelt gratitude to my thesis advisor, Dr. Ankur Goswami, for his invaluable guidance and the opportunities he has provided me, which will undoubtedly shape my future career. His encouragement to delve deeply into scientific research and pursue meaningful work, while granting me freedom to work independently and explore ideas with confidence, has been truly inspiring. During this journey, I had the privilege of spending considerable time working closely with Prof. Krishna Balasubramanian. His guidance played a crucial role in strengthening my understanding of fundamental concepts and deepening my overall perspective on the subject. Through his consistent insights, constructive feedback, and thoughtful discussions, he continually encouraged me to strive for higher standards and approach problems with greater clarity and rigor. His valuable mentorship and unwavering support throughout my work have been instrumental in shaping both my academic growth and the successful completion of this journey. Special thanks to my best friend, Jay Krishna Anand. Together, we tackled every challenge during my PhD tenure. His unwavering support and collaborative spirit were essential in overcoming the obstacles I faced throughout my doctoral journey. Also, I am profoundly grateful to my best friend and companion, Ms. Archana Verma. Her constant support and presence throughout my PhD tenure were essential in overcoming every challenge I faced. I truly value her unwavering dedication and companionship.

I also extend my heartfelt thanks to Prof. Sameer Sapra and Prof. Tapajyoti Das Gupta for granting me access to their laboratories and consistent discussions. Without their generous support, the successful conclusion of my research might not have been possible. I am extremely thankful to my SRC members Prof. Jayant Jain, Prof. Nitya nand Gosvami, and Prof. Sunil Kumar for their insightful suggestions, constructive criticisms, and invaluable guidance throughout my work. Their feedback greatly contributed to the improvement of my thesis research work. I equally thank to the Head of the Department

---

of Materials Science and Engineering, Prof. Jayant Jain for his invaluable feedback and encouragement. I am also deeply appreciative to the Department of Materials Science and Engineering for providing access to all the necessary facilities that enabled me to carry out my experiments effectively.

The journey of research is often challenging, but it is made significantly more enjoyable by the camaraderie and support of the lab fraternity. I am immensely grateful to my seniors—Dr. Shailendra Kumar and Mr. Sooraj who were always willing to extend their help and guidance. A special thanks to my labmates in the Advanced Materials System Laboratory: Dr. Rajesh Kumar Jha, Ms. Shalini Singh, Mr. Chhotrai Soren, Mr. Ujjwal Chitnis, Ms. Sonika Singh, Mr. Tarun Pratap Singh, Mr. Siddhanta, Mr. Tajamul Wani, Mr. Srest Somay, Ms. Rupali Srivastava and Ms. Approva for their support during this journey. Your unwavering support, encouragement, and camaraderie have been invaluable and have made this journey truly memorable. I am also profoundly thankful to my friends Dr. Udit Pant, Dr. Arvind, Mr. Sandeep, Mr. Dheeraj, Mr. Arun Sehrawat, Mr. Surajbhan Jaiswal, whose constant encouragement has been a source of strength throughout my doctoral studies. I acknowledge the generous financial support provided by the Ministry of Human Resource Development (MHRD), which has been instrumental in enabling my doctoral research.

I am deeply grateful to my parents, Mrs. Sada Pyari Verma and Mr. Shiv Balak Ram Verma. Their unwavering support and constant motivation have been the driving force behind my achievements, inspiring me to always strive for greatness. Finally, I extend my sincere gratitude to my family members for their unwavering love and support. To my uncle, Mr. Ram Narayan Verma and Mr. Ram Sevak Verma; my grandmother Mrs. Ketaki, my auntie, Mrs. Sushila Devi; my sisters, Mrs. Sangeeta, Mrs. Poonam, Mrs. Sarita, Mrs. Alpana and Mrs. Damini ; and my brothers, Mr. Ganesh Verma, Mr. Sailesh Verma - your love, encouragement, and faith in me have given me the strength to overcome challenges with courage and determination. I am grateful to you all for your tireless efforts and consistent belief in my success.

(Durgesh Banswar)

## ABSTRACT

The domain of nanoscale science and engineering presents how energy and matter behave at the atomic and molecular level, a scale where traditional physics often does not apply. At this scale, materials exhibit unique physical properties that deviate significantly from their bulk counterparts, opening pathways for revolutionary advancements in areas ranging from ultra-sensitive sensing and energy harvesting to quantum computing and advanced optoelectronic. To Unlock these potentials, One need to have a profound understanding of how various physical phenomena manifest and interect when dimensions shrink to the nanometer regime.

This thesis delves into this fascinating world by focusing on the important role of resonance. Resonance, in its fundamental forms: optical and mechanical provides a way for probing, enhancing, and controlling interactions within nanoscale systems. By integrating semiconductor materials with meticulously designed plasmonics and nanomechanical structures, this research aims to reveal complex physical behaviors and develop novel methodologies for characterization and device applications. One critical aspect of understanding materials at the nanoscale is the accurate determination of their mechanical properties. Traditional methods often prove inadequate for structures just a few nanometers thick or wide. Therefore, in the first work, thesis explores the measurement of Youngs modulus by utilizing resonance frequency via optical methods. This noncontact and highly sensitive approach leverages the precise relationship between a nanostructure's resonant frequency and its intrinsic mechanical stiffness. By optically exciting and detecting these minute oscillations, we can calculate fundamental mechanical parameters, providing crucial insights for designing robust and functional nanodevices.

Further, As the optical properties of the semiconductor materials are mainly influenced by quasi-particles such as excitons or trions, the bound states of electron-hole pairs (excitons) or charged electron-hole complexes (trions) which dictate light absorp-

---

tion and emission characteristics. This work investigates exciton-trion dynamics in semiconductor materials ( $\text{MoSe}_2$ ), particularly in the presence of plasmonic nanostructures. Plasmonic resonance in these metallic components creates a highly concentrated local electromagnetic fields that can strongly interact with charge carriers such as excitons and trions, modifying their generation, recombination, and energy transfer pathways. Understanding these light-matter interactions with plasmonics can assist in the development of high-performance nanoscale devices.

Finally, a significant challenge in the efficiency of optoelectronic devices based on perovskite nanocrystals exists known as the phonon bottleneck, which describes the hindered relaxation of energetic charge carriers or excitons due to a mismatch between their discrete electronic energy levels and the continuous phonon spectrum available for energy dissipation. The thesis will explore the implications of this bottleneck and further investigate the potential way to overcome or to minimise its effects by plasmonic interactions, thereby improving the overall efficiency of nanoscale systems.

Through interdisciplinary investigation, this thesis work provides a profound understanding of nanoscale phenomena governed by resonance. By developing and applying advanced optical characterization techniques for mechanical properties, demonstrating complex exciton-trion-plasmon interactions, and addressing the challenges of phonon-mediated energy relaxation, this research delivers a pathway for the implementation of next-generation semiconductor-based plasmonic and nanomechanical applications.

**Keywords:** Resonance frequency, mechanical resonance, optical resonance, quality factor, plasmons, exciton, trion, phonon-bottleneck.

---

## सारांश:

नैनोस्केल विज्ञान और इंजीनियरिंग का क्षेत्र अपार संभावनाओं की एक सीमा प्रस्तुत करता है, जो पदार्थ और ऊर्जा को उसकी मूलभूत सीमाओं पर हेरफेर करने के अभूतपूर्व अवसर प्रदान करता है। इस छोटे पैमाने पर, सामग्री अद्वितीय भौतिक गुण प्रदर्शित करती है जो अपने बड़े समकक्षों से काफी अलग होती है, जो अति-संवेदनशील संवेदन और ऊर्जा संचयन से लेकर क्वांटम कंप्यूटिंग और उन्नत ऑप्टोइलेक्ट्रॉनिक्स तक के क्षेत्रों में क्रांतिकारी प्रगति के लिए मार्ग खोलती है। इन संभावनाओं को अनलॉक करने के लिए इस बात की गहन समझ की आवश्यकता होती है कि जब आयाम नैनोमीटर शासन में सिकुड़ते हैं तो विभिन्न भौतिक घटनाएँ कैसे प्रकट होती हैं और परस्पर क्रिया करती हैं। यह थीसिस अनुनाद की महत्वपूर्ण भूमिका पर ध्यान केंद्रित करके इस आकर्षक दुनिया में प्रवेश करती है। अनुनाद, अपने असंख्य रूपों में - ऑप्टिकल, मैकेनिकल और इलेक्ट्रिकल नैनोस्केल सिस्टम के भीतर अंतःक्रियाओं की जांच, वृद्धि और नियंत्रण के लिए एक शक्तिशाली उपकरण प्रदान करता है। सावधानीपूर्वक डिज़ाइन किए गए प्लास्मोनिक्स और नैनोमैकेनिकल संरचनाओं के साथ अर्धचालक सामग्रियों को रणनीतिक रूप से एकीकृत करके, इस शोध का उद्देश्य जटिल भौतिक व्यवहारों को उजागर करना और लक्षण वर्णन और उपकरण अनुप्रयोगों के लिए नई पद्धतियाँ विकसित करना है। नैनोस्केल पर सामग्रियों को समझने का एक महत्वपूर्ण पहलू उनके यांत्रिक गुणों का सटीक निर्धारण है। पारंपरिक तरीके अक्सर कुछ नैनोमीटर मोटी या चौड़ी संरचनाओं के लिए अपर्याप्त साबित होते हैं। इसलिए, पहले कार्य में थीसिस ऑप्टिकल विधियों के माध्यम से अनुनाद आवृत्ति विश्लेषण का उपयोग करके यंग्स मापांक के मापन की खोज करती है। यह गैर-संपर्क और अत्यधिक संवेदनशील दृष्टिकोण नैनोस्ट्रक्चर की अनुनाद कंपन आवृत्ति और इसकी आंतरिक यांत्रिक कठोरता के बीच सटीक संबंध का लाभ उठाता है। ऑप्टिकल रूप से उत्तेजित करके और इन सूक्ष्म दोलनों का पता लगाकर, हम मूलभूत यांत्रिक मापदंडों का अनुमान लगा सकते हैं, जो मजबूत और कार्यात्मक नैनोडिवाइस डिजाइन करने के लिए महत्वपूर्ण अंतर्दृष्टि प्रदान करते हैं। इसके अलावा, नैनोस्केल पर अर्धचालक पदार्थों के ऑप्टिकल और इलेक्ट्रॉनिक गुण एक्साइटन और ट्रिऑन जैसे क्वासिपार्टिकल्स से गहराई से प्रभावित होते हैं। इलेक्ट्रॉन-होल युग्मों (एक्साइटन) या आवेशित इलेक्ट्रॉन-होल कॉम्प्लेक्स (ट्रिऑन) की ये बंधी हुई अवस्थाएँ प्रकाश अवशोषण और उत्सर्जन विशेषताओं को निर्धारित करती हैं। यह कार्य अर्धचालक पदार्थों में एक्साइटन-ट्रिऑन गतिशीलता की जांच करता है, विशेष रूप से प्लास्मोनिक नैनोस्ट्रक्चर की उपस्थिति में। इन धातु घटकों में स्थानीयकृत सतह प्लास्मोन अनुनाद अत्यधिक केंद्रित विद्युत चुम्बकीय क्षेत्र बनाते हैं जो एक्साइटन और ट्रिऑन के साथ दृढ़ता से बातचीत कर सकते हैं, उनकी पीढ़ी, पुनर्संयोजन और ऊर्जा हस्तांतरण मार्गों को संशोधित कर सकते हैं। इन जटिल प्रकाश-पदार्थ इंटरैक्शन को समझना और उनका उपयोग करना उच्च-प्रदर्शन नैनोस्केल ऑप्टोइलेक्ट्रॉनिक उपकरणों को विकसित करने की कुंजी है।

अंत में, नैनोस्केल ऊर्जा प्रबंधन और डिवाइस दक्षता में एक महत्वपूर्ण चुनौती, विशेष रूप से नैनोक्रीस्टल और

---

अन्य सीमित अर्धचालक प्रणालियों में, फोनन अड़चन है। यह घटना उनके असतत इलेक्ट्रॉनिक ऊर्जा स्तरों और ऊर्जा अपव्यय के लिए उपलब्ध निरंतर फोनन स्पेक्ट्रम के बीच बेमेल के कारण ऊर्जावान चार्ज वाहकों या एक्साइटन के बाधित विश्राम का वर्णन करती है। थीसिस इस अड़चन के निहितार्थों का पता लगाएगी और इसके प्रभावों को कम करने के लिए प्लास्मोनिक और नैनोमैकेनिकल इंटरैक्शन को शामिल करने वाली संभावित रणनीतियों की जांच करेगी, जिससे नैनोस्केल सिस्टम की समग्र दक्षता में सुधार होगा। इस अंतःविषय जांच के माध्यम से, इस थीसिस का उद्देश्य अनुनाद द्वारा शासित नैनोस्केल घटनाओं की मौलिक समझ में योगदान करना है। यांत्रिक गुणों के लिए उन्नत ऑप्टिकल लक्षण वर्णन तकनीकों को विकसित और लागू करके, जटिल एक्साइटन-ट्रियन-प्लास्मोन इंटरैक्शन को स्पष्ट करके, और फोनन-मध्यस्थ ऊर्जा विश्राम की चुनौतियों का समाधान करके, यह शोध अगली पीढ़ी के उच्च-प्रदर्शन अर्धचालक आधारित प्लास्मोनिक और नैनोमैकेनिकल उपकरणों के डिजाइन और कार्यान्वयन का मार्ग प्रशस्त करना चाहता है।

मुख्य शब्द: अनुनाद आवृत्ति, यांत्रिक अनुनाद, ऑप्टिकल अनुनाद, गुणवत्ता कारक, प्लास्मोन्स, एक्सिटोन, ट्रियोन, फोनोन-बॉटलनेक।।

# Contents

<b>CERTIFICATE</b>	<b>ii</b>
<b>ACKNOWLEDGEMENTS</b>	<b>iii</b>
<b>ABSTRACT</b>	<b>v</b>
<b>List of Figures</b>	<b>xiii</b>
<b>List of Tables</b>	<b>xix</b>
<b>List of Abbreviations</b>	<b>xx</b>
<b>List of Symbols</b>	<b>xxii</b>
<b>1 Introduction</b>	<b>1</b>
1.1 Resonance in the Nanoscale Systems: A Foundational Concept . . . . .	1
1.1.1 Acoustic Resonance . . . . .	2
1.1.2 Electrical Resonance . . . . .	2
1.1.3 Magnetic Resonance . . . . .	2
1.1.4 Mechanical Resonance . . . . .	3
1.1.4.1 Nanomechanical resonator . . . . .	3
1.1.5 Optical Resonance . . . . .	5
1.1.5.1 Fabry-Perot cavity . . . . .	5
1.1.5.2 Ring resonator . . . . .	5
1.1.5.3 Photonic Crystal cavity - PNC . . . . .	6
1.1.5.4 Plasmonics . . . . .	6
<b>2 Literature Survey</b>	<b>8</b>

2.1	Nanomechanical Devices . . . . .	8
2.1.1	Mechanical Resonance at Nanoscale regime: A Brief History . .	8
2.1.2	Nanomechanical Resonance . . . . .	9
2.1.3	Evolution of Micro-Cantilever based sensors . . . . .	10
2.1.3.1	Microcantilever Resonator : SHM Model . . . . .	10
2.1.3.2	Euler-Lagrange Model . . . . .	13
2.1.3.3	Quality factor . . . . .	15
2.1.4	Applications . . . . .	15
2.1.4.1	Mass sensors . . . . .	15
2.1.4.2	Material Characterization (Youngs Modulus Measurement)	16
2.2	Employing Optical resonance : Surface Plasmons . . . . .	17
2.2.1	Plasmons in metal Nanoparticles : A Brief History . . . . .	17
2.2.2	Plasmonic Resonance . . . . .	18
2.2.3	Plasmonic devices . . . . .	18
2.2.3.1	The Drude Model . . . . .	19
2.2.3.2	Lorentz Oscillator Model . . . . .	21
2.2.3.3	Drude-Lorentz Model . . . . .	23
2.2.3.4	Local Surface Plasmon Resonance : LSPR . . . . .	23
2.2.4	Emerging Plasmomic Device: Gallium Nanodroplets . . . . .	25
2.2.5	Application . . . . .	25
2.2.5.1	2D Material (MoSe <sub>2</sub> ): Enhanced by LSPR . . . . .	26
2.2.5.2	Perovskite Material (FAPbBr <sub>3</sub> ): Enhanced by LSPR . . .	27
2.3	Motivation . . . . .	29
2.4	Objectives of Thesis . . . . .	30
2.5	Thesis Overview . . . . .	30
<b>3</b>	<b>Resonance Frequency Measurement Unit (RFMU) for the Dynamic charac-</b>	
	<b>terization of Nanomechanical Resonator</b>	<b>33</b>
3.1	Introduction . . . . .	33
3.2	Experimental Setup and Working Mechanism of RFMU . . . . .	34
3.3	Experimental Results . . . . .	35
3.3.1	Instrument mechanism . . . . .	35

---

3.3.2	Measurement Results . . . . .	37
3.3.3	Theoretical Analysis . . . . .	40
3.3.4	Comparative Analysis . . . . .	44
3.4	Conclusions . . . . .	45
<b>4</b>	<b>Non-destructive evaluation of Youngs modulus of materials using dynamic-optical technique</b>	<b>46</b>
4.1	Introduction . . . . .	46
4.2	Experimental Method . . . . .	48
4.2.1	Optical Technique . . . . .	48
4.2.2	Materials and characterization . . . . .	48
4.3	Results and Discussion . . . . .	49
4.3.1	Methods . . . . .	49
4.3.2	Experimental Results . . . . .	53
4.3.2.1	HEA thin film . . . . .	53
4.3.2.2	VO <sub>2</sub> thin film . . . . .	53
4.4	Discussions . . . . .	54
4.5	Conclusions . . . . .	56
<b>5</b>	<b>On the unique temperature-dependent interplay of a B-exciton and its trion in monolayer MoSe<sub>2</sub></b>	<b>58</b>
5.1	Introduction . . . . .	58
5.2	Experimental Methods . . . . .	60
5.3	Results . . . . .	62
5.4	Discussions . . . . .	69
5.5	Conclusion . . . . .	72
<b>6</b>	<b>Exciton-Phonon-Plasmon Interplay in Hot Carrier Relaxation Dynamics in Perovskite Crystals</b>	<b>74</b>
6.1	Introduction . . . . .	74
6.2	Experimental Methods . . . . .	76
6.3	Computational Methodology . . . . .	78
6.4	Results . . . . .	78
6.4.1	Exciton-Phonon-Plasmon Interactions . . . . .	83

6.5	Discussions . . . . .	88
6.5.1	Exciton-Plasmon-Phonon interplay . . . . .	89
6.6	Conclusion . . . . .	90
<b>7</b>	<b>Conclusions and Future Perspectives</b>	<b>91</b>
7.1	Conclusions . . . . .	91
7.2	Future Aspects . . . . .	92
	<b>References</b>	<b>93</b>
	<b>Appendix 1</b>	<b>108</b>
1	Temperature dependent resonance frequency . . . . .	108
2	Comparative Analysis with LDV . . . . .	110
	<b>Appendix 2</b>	<b>111</b>
1	Sample Preparation . . . . .	111
2	Optical Characterization . . . . .	111
3	GPNS - time dependent measurements . . . . .	112
4	FEM Calculations . . . . .	113
5	FEM calculations with variation in size and separations . . . . .	114
	<b>Appendix 3</b>	<b>117</b>
1	Sample Preparation . . . . .	117
2	Optical Characterization . . . . .	118
3	SEM . . . . .	119
4	XRD . . . . .	120
5	Low temperature analysis and quantum yield . . . . .	121
6	TRPL . . . . .	124
7	Transient absorption . . . . .	125
8	DFT calculations . . . . .	126
	<b>List of Publications</b>	<b>127</b>

## List of Figures

1.1	Schematic of Nanomechanical devices (A) microstring, (B) microdrum, (C) micromirror, and (D) microcantilever. [13][27][5][29] . . . . .	4
1.2	Schematic of plasmonics devices (A) nanorods, (B) nanocubes, (C) nanoholes, and (D) nanodroplets. [40][39][41][43] . . . . .	6
2.1	(A) Schematic for light-matter interaction in MoSe <sub>2</sub> and Gallium nanodroplets interfaces. . . . .	26
2.2	Schematic of MoSe <sub>2</sub> (A) monolayer, (B) Multilayer . . . . .	27
2.3	(A) Schematic for light-matter interaction in FAPbBr <sub>3</sub> and Gallium nanodroplets interfaces. . . . .	28
2.4	Schematic for Crystal structure of perovskite materials (ABX <sub>3</sub> ). . . . .	29
3.1	(A) Ray diagram of the inhouse build instrument (RFMU), integrated with the heating stage and temperature controller, (B) schematic of the instrument. . . . .	36
3.2	SEM image of microcantilever devices (A) M <sub>1</sub> , (B) M <sub>2</sub> , (C) M <sub>3</sub> , resonance frequency with corresponding phase spectra of devices (D) M <sub>1</sub> , (E) M <sub>2</sub> and (F) M <sub>3</sub> fitted with the Lorentzian function at ambient conditions (red curve) and in vacuum conditions (blue curve), noise calibration of devices (G) M <sub>1</sub> , (H) M <sub>2</sub> and (I) M <sub>3</sub> in air (red curve) and vacuum conditions (black curve). . . . .	38
3.3	Resonance frequency spectra of microcantilever devices M <sub>1</sub> , M <sub>2</sub> and M <sub>3</sub> respectively with temperature variation shows; (A) Spectra at 30 °C, (B) 60 °C, (C) 80 °C, (D) 100 °C, (E) 140 °C and (F) 180 °C. . . . .	39
3.4	Resonance frequency spectra with temperature variation at ambient pressure for (A) M <sub>1</sub> , (B) M <sub>2</sub> and (C) M <sub>3</sub> . . . . .	40
3.5	Resonance frequency spectra of microcantilever device measured with (A) RFMU and (B) LDV . . . . .	44
4.1	Schematic of the technique used to measure the Young's modulus of thin films. . . . .	49

4.2	(A) XRD spectra of VO <sub>2</sub> M phase and (B) corresponding AFM image of the surface of the VO <sub>2</sub> thin film, (C) XRD spectra of HEA and corresponding (D) surface morphology of the (AlCoCrFeNi) <sub>0.2</sub> thin film. . . . .	50
4.3	(A) Schematic of bare microcantilever (B <sub>1</sub> ) of dimensions (l,b,h) and HEA coated microcantilever device, (B) bare microcantilever (B <sub>2</sub> ) of dimensions (l,b,h) and corresponding VO <sub>2</sub> coated microcantilever device (C) SEM image of microcantilever device (B <sub>1</sub> ) used for HEA with inset showing morphology of HEA coated device and (D) image of microcantilever device (B <sub>2</sub> ) used for VO <sub>2</sub> with inset showing morphology of VO <sub>2</sub> coated device. . . .	51
4.4	(A) Resonance frequency spectra of Bare microcantilever (B <sub>1</sub> ) at different temperatures varying from 20 °C to 200 °C, (B) Resonance frequency spectra of HEA coated microcantilever device at temperatures varying from 20 °C to 200 °C, (C) temperature dependent resonance frequency of bare cantilever and (D) with HEA coated at temperature ranges from 20 °C to 200 °C. . . . .	54
4.5	(A) Resonance frequency spectra of bare microcantilever (B <sub>2</sub> ) at different temperatures varying from 20 °C to 200 °C, (B) Resonance frequency spectra of VO <sub>2</sub> coated microcantilever device at temperatures varying from 20 °C to 200 °C, (C) temperature dependent resonance frequency of bare cantilever and (D) with VO <sub>2</sub> coated at temperature ranges from 20 °C to 200 °C. . . . .	55
4.6	(A) Young's Modulus of HEA thin film at different temperatures varying from 20 °C to 200 °C, (B) Young's Modulus of VO <sub>2</sub> thin film at different temperatures varying from 20 °C to 150 °C. . . . .	56
5.1	(A) Process flow of thermal evaporation method to develop nanoengineered substrate, (B) FESEM image of arrays of grown Ga particles over glass substrate with MoSe <sub>2</sub> flakes suspended. . . . .	61
5.2	(A) Raman spectra of as prepared MoSe <sub>2</sub> nanoflakes (blue curve) and Raman spectra of MoSe <sub>2</sub> deposited over Ga nanodroplets of radius 100 nm (Red curve) which shows 2-fold enhancement in the dominant vibrational modes of MoSe <sub>2</sub> , (B) UV-Vis absorption spectra of as prepared MoSe <sub>2</sub> nanosheets with absorption peaks at 790 nm, 695 nm and 460 nm corresponding to A exciton, B exciton and C exciton deconvoluted with Gaussian function, (C) Simulated absorption spectra of MoSe <sub>2</sub> -Ga with COMSOL Multiphysics tool for gallium droplet radius of 100 nm (GPNS-100) and 150 nm (GPNS-100), (D) Reflectivity spectra of monolayer of MoSe <sub>2</sub> over GPNS showing a characteristic extinction near 704 nm (B exciton) for GPNS-100 and characteristic extinction near 738 nm and 789 nm for GPNS-100. . . . .	63

- 
- 5.3 (A) PL spectra of as prepared samples of MoSe<sub>2</sub> flakes on glass substrate at room temperature (white starred curve) and PL of MoSe<sub>2</sub> on nanoengineered substrate (MoSe<sub>2</sub>-GPNS) shown with black starred curve, well deconvoluted with Gaussian function for exciton and trion peaks (red curve shows B exciton position and blue curve shows B trion position), (B) PL spectra of MoSe<sub>2</sub> with Ga droplet size of 100 nm (white curve) and 150 nm (black curve) respectively, (C) Schematic of plasmonic mode coupling with B exciton and trions. . . . . 65
- 5.4 (A) Photoluminescence spectra of as prepared MoSe<sub>2</sub> on nanoengineered substrate (MoSe<sub>2</sub>-GPNS) at low temperature ranges from 100 K to 300 K, (B) to (E) Gaussian curve fit for exciton and trion peaks at individual temperatures from 100 K to 300 K. . . . . 66
- 5.5 (A) Dependency of emission energy corresponding to the position of B excitons peak with temperature and inset shows (relative fall in the peak position for B exciton and trion with temperature), (B) Trion peak dependency with temperature range from 100 K to 300 K. Continuous red line is fitted curve having parameters  $E_B = 1.76$  eV,  $A_B = 68$  meV/K for B exciton and  $E_B = 1.69$  eV,  $A_B = 11$  meV/K for trion, (C) Dependency of Integrated Intensity corresponding to the B excitonic peak and inset shows (relative intensity variation in B exciton and trion with temperature range from 100 K to 300 K), (D) Integrated intensity variation of trion with temperature range from 100 K to 300 K. Parameters for the fit curves in solid lines in (C) and (D) show that the most dominant energy mode is 32 – 36 meV, pointing at the most dominant  $A_{1g}$  phonon. . . . . 68
- 5.6 (A) Temperature dependency of trion binding energy (red starred curve) with inset showing (normalized experimental in blue line and simulated pattern in red dotted lines) and (B) Intensity ratio of exciton with trion (red starred curve) with temperature ranges from 100 K to 300 K (simulated results (black continuous line) closely matches with experimental pattern as shown in inset), (C) Schematic of trion formation process at temperatures at 300 K and (D) at 100 K with  $\nu$  being the average electron energy above the conduction band minimum and  $E_B^-$  is the actual 0 K exciton-trion binding energy. Color gradient represents the density of carriers. . . . . 70
- 6.1 Electron microscope image of Gallium nanodroplets over glass substrate deposited with inset showing the particle size distributions (B) FAPbBr<sub>3</sub> NCs over glass substrate with inset showing the particle size distribution, (C) FAPbBr<sub>3</sub> NC over Ga nanodroplets where the NC is highlighted using false color and inset showing NCs size distribution. . . . . 79
-

- 
- 6.2 Raman spectra of NCs and Ga-NCs showing dominant phonon band of 65.09 meV, (B) Absorption spectra of NC and Ga: NC with Tauc plot for optical bandgap inset showing band edge at 557 nm, (C) photoluminescence spectra of NC and Ga: NC with excitation wavelength 440 nm at RT (D) excitation energy dependent photoluminescence (EPL) trend of NC and (E) with Ga-NC with inset showing EPL spectra at excitation wavelength 375 nm to 500 nm, (F) Maximum  $I_{PL}$  intensity variation with excitation wavelength of NC and Ga-NC. . . . . 80
- 6.3 Temperature dependent photoluminescence spectra of (A) NC (FAPbBr<sub>3</sub>) and (B) Ga: FAPbBr<sub>3</sub> from 10 K to 300 K with 3D spectrum along with color map that indicates the shift in peak center and the shape with temperature (C) The exact trends in peak position of NC and Ga-NC showing similar red shift at lower temperatures (inset shows a noticeable 40K lower perovskite phase change temperature on the Ga-NC). (D) Temperature dependent integrated PL intensity ( $I_{PL}$ ) spectra of NC and Ga-NC with inset showing the  $I_{PL}$  ratio at different temperatures exposing the non-monotonic behaviour. . . . . 81
- 6.4 Time dependent PL profile NCs and Ga-NCs when the samples were excited at 375 nm. A two orders of magnitude faster decay in Ga-NC is observed due to possible removal of phonon blockade (B) When the samples were excited at slightly lower energy (440 nm) a starker difference in the decay dynamics is noted.(C) When excited at bandedge ( 532 nm) where intraband relaxations are not needed, both the samples decay similarly.(D) Decay dynamics spectra of the prepared FAPbBr<sub>3</sub> crystals with varying fluence power of the pump source, showing faster decay lifetime of carriers at low pump power (9  $\mu$ J.cm<sup>-2</sup>), (E) Decay dynamics of carriers in Ga-NCs showing no change in lifetime decay with pump power at 375 nm excitation wavelength, (F) Schematic representation of excitation positions, (G) transient absorbance spectra of NCs and (H) Ga-NCs showing as surface plots and (I) average lifetime of carriers of NCs (black curve: 7.5 ns) and Ga-NCs (red curve: 650 ps) shows carrier decay dynamics at maximum absorbance position (551 nm for NCs and 545 nm for Ga-NCs) probed at 440 nm energy and inset shows change in transient absorbance at 200fs with NC and Ga-NC demonstrating higher absorbance of Ga-NC above the band-edge energy. . . . . 84
- 6.5 Schematic of relaxation mechanism in NCs and Ga-NCs with 375 nm and 440 nm excitation wavelength and (B) near band edge position (532 nm), (C) Carrier density relaxation for NCs (shown with black curve) and Ga-NCs (inset – red curve) at 375 nm wavelength excitation. (D) Band-edge carrier density relaxation for Ga-NC or NC (both having same trend) at 532 nm wavelength excitation and photoluminescence spectrum of Ga and Ga-NC with excitation close to band-edge position (532 nm), (E) Calculated average occupation energy spectra of NCs and Ga-NCs showing blue shift of 54.3 meV (equals to the 13 nm blue shift with Ga-NCs). . . . 87
-

A1	(A) Preparation of GPNS substrate with thermal evaporated technique, (B) schematic for Gallium based plasmonic Nano-substrates (GPNS), (C) MoSe <sub>2</sub> solution in toluene after sonication, (D) schematic of MoSe <sub>2</sub> on top of the GPNS substrate. . . . .	112
A2	(A) Schematic for measurement of reflectance of MoSe <sub>2</sub> -GPNS in UV-vis with integrating sphere assembly, (B) Direct detection unit for absorption measurement of MoSe <sub>2</sub> over glass substrate (BS is beam splitter and M is denoted for Mirror). . . . .	113
A3	(A) Raman spectra of MoSe <sub>2</sub> -GPNS with gallium droplet radius of 100 nm and 150 nm, (B) time dependent PL spectra of MoSe <sub>2</sub> -GPNS with excitation wavelengths of 485 nm and 532 nm. . . . .	114
A4	Light-matter interaction between gallium nanoparticles and MoSe <sub>2</sub> monolayer at B and A exciton positions for-radius of particle to be 100 nm and radius of Ga particles to be 150 nm. . . . .	115
A5	calculated absorbance spectra of Ga-MoSe <sub>2</sub> with radius of particles (100 – 175) nm. . . . .	116
A6	Stepwise preparation procedure of FAPbBr <sub>3</sub> crystals. . . . .	117
A7	(A) Preparation of Ga nanodroplets on glass substrate with thermal evaporation method, (B) Prepared Ga nanodroplets over glass substrate, (C) Solution of FAPbBr <sub>3</sub> and PbBr <sub>2</sub> for the preparation of FAPbBr <sub>3</sub> NCs (D) Schematic of morphology of FAPbBr <sub>3</sub> over Ga nanodroplets. . . . .	118
A8	Schematic for measurement of Absorbance in UV-vis with integrating sphere assembly. . . . .	119
A9	(A) SEM image of Ga-NCs, (B) EDS image of the Ga-NCs and corresponding (C) EDS mapping of the elements showing dominant presence of Ga and FAPbBr <sub>3</sub> or (CH <sub>3</sub> NH <sub>2</sub> ) <sub>2</sub> PbBr <sub>3</sub> . . . . .	120
A10	XRD spectra of the prepared FAPbBr <sub>3</sub> (NC) nanocrystals (black curve) and XRD spectra of Ga-NCs (red curve) showing same crystallographic structure at room temperature with minor humps due to excess scattering in Ga substrates. . . . .	121
A11	(A) Schematic representation of recombination pathways (P1 and P2) for NCs and Ga-NCs suggesting excess occupation rate in Ga-NCs as compared to NCs, (B) full width half maxima (FWHM) spectra of NCs and Ga-NCs at temperatures 10K to 300K fitted with Segal's model, suggesting broadening in PL spectrum of Ga-NCs, hence justifying schematic A. . .	124
A12	(A) Decay dynamics spectra of the prepared FAPbBr <sub>3</sub> crystals with varying fluence power of the pump source, showing faster decay lifetime of carriers at low pump power (9 μJ.cm <sup>-2</sup> ), (B) Decay dynamics of carriers in Ga-NCs showing no change in lifetime decay with pump power at 375 nm excitation wavelength. . . . .	125

A13	Differential absorbance curve of (A) NC and (B) Ga-NC with 440 nm pump energy. . . . .	125
A14	Phonon dispersion and corresponding density of states calculated using DFT (A) FAPbBr <sub>3</sub> and (B) Ga-FAPbBr <sub>3</sub> . . . . .	126

## List of Tables

1.1	Comparison between plasmonic devices . . . . .	7
2.1	Application of Microcantilever resonator . . . . .	11
5.1	parameters of MoSe <sub>2</sub> monolayer on glass substrate and MoSe <sub>2</sub> on GPNS-100 (PL) . . . . .	69
6.1	Parameters for relaxation mechanism . . . . .	88
A1	Dynamic properties of devices (M <sub>1</sub> , M <sub>2</sub> , M <sub>3</sub> ) at ambient conditions . . . . .	109
A2	Comparison of resonance frequency measurement techniques for microcantilever devices . . . . .	110
A3	Optical response of nanoparticles at different sizes . . . . .	114
A4	Phonon contribution in gallium-perovskite composite. . . . .	123
A5	Decay lifetimes at different fluence powers for FAPbBr <sub>3</sub> and Ga-FAPbBr <sub>3</sub> . . . . .	124

## List of Abbreviation

<b>AFM</b>	Atomic Force Microscopy
<b>Ag</b>	Silver
<b>Au</b>	Gold
<b>C.B</b>	Conduction Band
<b>DMF</b>	Dimethylformamide
<b>EDS</b>	Energy Dispersive X-ray Spectroscopy
<b>ETR</b>	Exciton Trion Intensity Ratio
<b>FAPbBr<sub>3</sub></b>	Formamidinium Lead Bromide
<b>FEM</b>	Finite Element Method
<b>FESEM</b>	Field Enhanced Scanning Electron Microscopy
<b>FWHM</b>	Full Width Half Maximum
<b>Ga</b>	Gallium
<b>GGA</b>	Generalized Gradient Approximation
<b>GPNS</b>	Gallium Based Plasmonic Nanosubstrates
<b>HEA</b>	High Entropy Alloy
<b>LDV</b>	Laser Doppler Vibrometer
<b>LEDs</b>	Light Emitting Diodes
<b>LO</b>	Lorentz Oscillator
<b>LPF</b>	Low Pass Filter
<b>LSPR</b>	Local Surface Plasmon Resonance
<b>MEMS</b>	Micro Electromechanical Systems

<b>MoSe<sub>2</sub></b>	Molybdenum Diselenide
<b>NCs</b>	Nanocrystals
<b>NEMS</b>	Nano Electromechanical Systems
<b>NTP</b>	Normal Temperature Pressure
<b>PL</b>	Photoluminescence Spectroscopy
<b>PNC</b>	Photonic Crystal Cavity
<b>RFMU</b>	Resonance Frequency Measurement Unit
<b>RN</b>	Exciton Radiative Recombination Rate
<b>SEM</b>	Scanning Electron Microscopy
<b>SERS</b>	Surface Enhanced Raman Spectroscopy
<b>SHM</b>	Simple Harmonic Oscillator Model
<b>SPs</b>	Surface Plasmons
<b>TA</b>	Transient Absorbance
<b>TCSPC</b>	Time Correlated Single Photon Counting
<b>TMD</b>	Transition Metal Dichalcogenide
<b>UV-vis</b>	Ultraviolet Visible
<b>VO<sub>2</sub></b>	Vanadium Di Oxide
<b>WLC</b>	White Light Continuum

## List of Symbols

$k_{eff}$	stiffness
$\phi$	Phase
$Q$	Quality factor
$\omega$	frequency
$I$	moment of inertia
$\rho$	density
$T$	Temperature
$\gamma$	damping coefficient
$H(\omega_{id,\eta})$	hydrodynamic load function
$A_{ex}$	A exciton
$B_{ex}$	B exciton
$B_{tr}$	A trion
$E_g(eV)$	Bandgap energy
$\chi_B$	exciton-trion energy difference
$E_B^-$	intrinsic B trion binding energy
$E_F(eV)$	Fermi energy
$N$	exciton density
$R_N$	exciton radiative recombination rate
$R_{TF}$	exciton to trion scattering rate
$P$	vacant phonon density of states
$R_{NRT}$	trion non-radiative recombination rate
$D$	total available phonon density of states
$c_e$	ionized electron density in conduction band
$T_r$	Trion density
$X_{BE}$	population of carriers at bandedge

$X_E$	excited carriers
$D_{LO}$	phonon density of states
$E_c$	conduction band edge energy
$E_{th}$	thermal energy
$L_o$	occupied optical phonon states
$T_{NR}$	intraband recombination rate
$G$	generation rate
$R$	radiative recombination rate
$NR$	non radiative recombination rate
$KC$	Klemen's channe